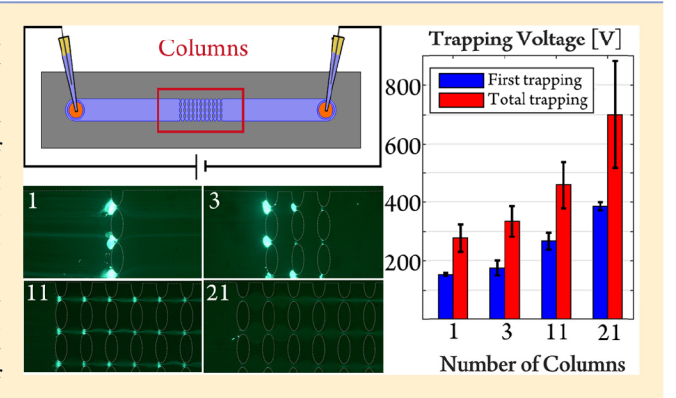


# Simple Approach to Reducing Particle Trapping Voltage in Insulator-**Based Dielectrophoretic Systems**

Victor H. Perez-Gonzalez,<sup>†,‡</sup> Roberto C. Gallo-Villanueva,<sup>†,‡</sup> Braulio Cardenas-Benitez,<sup>‡</sup> Sergio O. Martinez-Chapa,<sup>‡</sup> and Blanca H. Lapizco-Encinas<sup>\*,§</sup>

Supporting Information

ABSTRACT: Insulator-based dielectrophoresis (iDEP) is a microfluidic technique used for particle analysis in a wide array of applications. Significant efforts are dedicated to improve iDEP systems by reducing voltage requirements. This study assesses how the performance of an iDEP system, in terms of particle trapping, depends on the number of insulating obstacles longitudinally present in the microchannel. In analogy with Kirchhoff's loop rule, iDEP systems were analyzed as a series combination of electrical resistances, where the equivalent resistance of the post array is composed by a number of individual resistors (columns of insulating posts). It was predicted by the COMSOL model, and later confirmed by experimental results, that reducing the number of columns of insulating posts significantly affects the electric field distribu-



tion, decreasing the required voltage to dielectrophoretically trap particles within the post array. As an application, it was demonstrated that decreasing the number of columns in the post array allows for the dielectrophoretic trapping of nanometerscale particles at voltages well below those reported in previous similar iDEP systems. These findings illustrate how the iDEP channel configuration can be customized for specific applications.

ielectrophoresis (DEP) is the migration of particles due to particle polarization effects in the presence of a nonuniform electric field. Dielectrophoresis-based systems employ either electrodes and/or insulators to create the nonuniform electric fields required for the generation of dielectrophoretic forces.<sup>1,2</sup> Insulator-based dielectrophoresis (iDEP) is an electrokinetic microfluidic technique that is continuously gaining popularity in several fields, from biomedical assessments  $^{3-6}$  to bioanalysis.  $^{7-10}$ 

Usually, in iDEP devices 3-dimensional insulating structures are embedded in a microchannel and nonuniform electric fields are generated by applying an electric potential difference across the length of the microchannel. The presence of the insulating structures distorts the otherwise uniform electric field distribution, which in turn creates nonuniform polarization effects on particles. Effective particle manipulation is achieved when the dielectrophoretic force induced on the particles overcomes, or is at least comparable in magnitude to, all other forces acting on the particles. II Common microchannel designs include an array of insulators, i.e. posts, and particle trapping sites are generated within the post array. Several studies by our group 11-13 and others 2,14-17 have analyzed iDEP systems with the aim of improving performance, efficiency, and overall system design. Of particular interest is reducing the voltage requirement in iDEP systems by modifying the characteristics of the microchannel and insulating posts. Previous works have accomplished this through the integration of microfabricated electrodes in iDEP devices. 18,19 With this approach, the distance between electrodes can be significantly reduced, generating high electric fields with low applied voltages. Lowering the applied voltage not only decreases the generation of undesirable effects such as electrolysis and Joule heating but also reduces the footprint and complexity of the required electrical equipment.<sup>20±22</sup>

An essential concept related to iDEP systems is the distribution of the electric field across the length of a microchannel, which contains both the 3-dimensional insulating structures and the suspending medium. In the case of the traditional iDEP channels, as proposed by Cummings and Singh,<sup>23</sup> an increase in the size of insulating post arrays within the channel results in more potential trapping zones where particles can be dielectrophoretically immobilized. However, despite the importance of this finding, no study to date has explored how the magnitude of dielectrophoretic forces (and

Received: January 10, 2018 Accepted: March 12, 2018 Published: March 12, 2018

<sup>&</sup>lt;sup>‡</sup>School of Engineering and Sciences, Sensors and Devices Research Group, Tecnologico de Monterrey, Monterrey, Nuevo Leon

<sup>§</sup>Microscale Bioseparations Laboratory, Rochester Institute of Technology, Rochester, New York 14623, United States

thus, the overall trapping efficiency) changes as a function of the number of insulating posts in the array.

The present contribution studies the effect that the number of columns of insulating structures has on the electrokinetic forces exerted on particles in an iDEP microdevice. Four distinct iDEP channel designs were studied with 1, 3, 11, and 21 columns of insulating posts. A mathematical model was created in COMSOL Multiphysics to assess how the distribution of the electric potential, electric field, and gradient of electric field square depends on the number of columns of insulating posts in the microchannel. The model was validated by experimentation with 200 nm and 1  $\mu$ m polystyrene particles. The experimental results demonstrated that the number of the insulating posts within an iDEP system has a strong effect on the dielectrophoretic capture of particles. Voltage requirements to capture particles with DEP change dramatically as a function of channel configuration. By employing the device with the least number of insulating posts, it was possible to capture nanoparticles at highly reduced voltages. These findings illustrate how iDEP channel configuration can be customized for specific applications, in this case, for the capture of challenging nanoparticles at reduced voltages. These results open the possibility for iDEP systems to be used for the detection and enrichment of nanosized target particles, such as biomarkers, virus, and cell organelles.

#### ■ THEORY AND COMPUTATIONAL MODEL

Dielectrophoresis is the electrokinetic phenomenon that allows manipulating polarizable particles suspended in a fluidic medium through the generation of a spatially nonuniform electric field.<sup>24</sup> Dielectrophoresis depends, for the most part, on three different parameters: the size of the particle, the dielectric properties (*i.e.*, conductivity and permittivity) of the particle and suspending medium, and the spatial distribution of the electric field.<sup>25</sup> The dielectrophoretic force acting on a spherical polarizable particle suspended in solution is defined as

$$\mathbf{F}_{\text{DEP}} = 2\pi a^3 \epsilon_m \text{Re}\{K\} \nabla |\mathbf{E}|^2$$

where a is the particle radius,  $\varepsilon_m$  is the suspending medium permittivity, K is the complex Clausius—Mossotti factor (which accounts for particle-medium polarizability effects), and E is the electric field vector. The Clausius—Mossotti factor, which accounts for particle polarizability, is described by the relation:

$$K = \frac{\varepsilon_p^* - \varepsilon_m^*}{\varepsilon_p^* + 2\varepsilon_m^*} \tag{2}$$

with  $\varepsilon^* = \varepsilon - j\sigma/\omega$ . The subscripts p and m indicate particle and suspending medium, respectively, j is the imaginary number,  $\sigma$  is the conductivity, and  $\omega$  the angular frequency of the applied voltage ( $\omega = 0$  in DC-stimulated iDEP devices). 26,27 The distribution of the electric potential  $(\varphi)$ within the microfluidic channel defines the electric field that induces the dielectrophoretic force on the particles as E = $-\nabla \varphi$ . However, the value of  $\varphi$  at every point in the microfluidic device depends not only on the length of the channel, the shape of the insulating obstacles, and the applied voltage  $(\varphi_{inlet})$  but also on the number of columns of insulating posts within the microfluidic channel. Figure 1a presents a schematic representation of one such device. In our study, four distinct channel configurations were employed with varying number of columns of insulating posts: 1, 3, 11, and 21 columns (Figure S1). If each column of posts is modeled as an

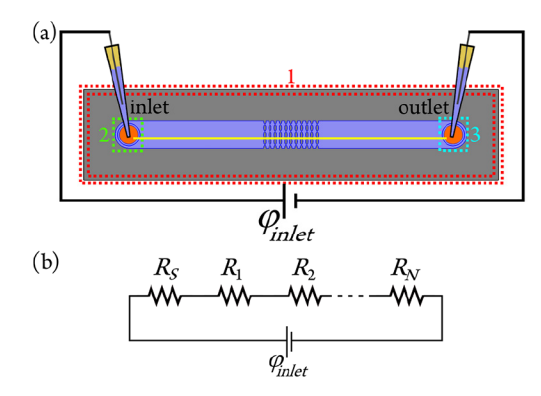


**Figure 1.** (a) Representation of one of the four microchannel designs used in this work. The dotted boxes identify boundaries, and distinctly colored regions identify the different domains used in the computational model. The yellow line depicts the cutline used for simulation estimations. (b) Schematic representation of an iDEP microchannel as an equivalent DC circuit.

electric resistor,  $R_i$ , it follows that a microfluidic channel with N columns can be modeled as a series combination of resistors, as illustrated in Figure 1b, with an equivalent resistance given by the expression:

$$R_{eq} = R_s + \sum_{i=1}^{N} R_i \tag{3}$$

where  $R_s$  and  $R_i$  represent the suspending solution resistance and the ith column resistance, respectively. Therefore, microfluidic designs with a large number of posts columns will exhibit greater equivalent resistance than those with a small number of posts columns. Furthermore, given Kirchhoff's loop rule,  $\phi \mathbf{E} \cdot \mathbf{ds}$ = 0, the sum of the voltage drops across a closed loop is zero. Specifically, the sum of all voltage drops along the microfluidic channel must be equal to the applied stimulation voltage,  $\varphi_{inlet}$ . Therefore, the voltage drop across a microfluidic channel containing only one column of insulating posts on its design will be much more abrupt than that which takes place in a design containing many more columns. This will translate into a stronger electric field, larger field spatial nonhomogeneity, and finally, a stronger induced dielectrophoretic force. Because each column of insulating posts can be modeled as a parallel combination of resistors, the electric potential drop across each post on the column is assumed to be the same. Adding or removing rows of posts to the design will not significantly alter particle trapping performance.

In order to study the spatial distribution of the electric field, computational models were built in COMSOL *Multiphysics* 5.2 (COMSOL Inc., Burlington, MA). The electric current module was used to solve the Laplace equation in a stationary study and obtain the distribution of electric potential (considering  $\varphi_{inlet}$  = 1000 V), throughout the devices. This allows calculating the electric field and the electric field square gradient, the latter directly proportional to the dielectrophoretic force.

For each design, a two-dimensional (2D) model was built, where the channel length (from reservoir center-to-center) and width are 10.16 mm and 850  $\mu$ m, respectively. The fabricated insulating obstacles consist of elliptical posts with a minor axis (x) of 75  $\mu$ m and a major axis (y) of 188  $\mu$ m. The spacing between posts is 90  $\mu$ m in the x-direction and 24.5  $\mu$ m in the y-direction. A column of posts is formed by three posts aligned in the y-direction and two half-posts, each located at the top and

bottom of the column, respectively. Designs differ only in the number of columns present in the channel (Figure S1).

Three different domains were defined in each model, and they are indicated with colored regions in Figure 1. Gray zones represent poly(dimethylsiloxane) (PDMS), blue zones represent water, orange zones represent platinum electrodes. Except for PDMS conductivity,  $\sigma_{PDMS}$ , and water conductivity,  $\sigma_{H_2O}$ , which were set to 2.5 × 10<sup>-14</sup> S/m and 5.5 × 10<sup>-6</sup> S/m, respectively, all material properties employed in the model were obtained from the COMSOL Material Library. Domain and boundary conditions used in the computational model are listed in Table S1. To solve the model, free triangular meshes were used with maximum and minimum element sizes of 130 and 0.261  $\mu$ m, respectively.

#### EXPERIMENTAL SECTION

**Microdevices.** Four distinct microchannel designs were employed in this study (Figure S1). Devices were fabricated in PDMS using conventional soft-lithography procedures listed in previous reports by our group. <sup>30,31</sup> The final dimensions of the fabricated devices are as mentioned in the Theory and Computational Model Section.

**Microparticles and reagents.** For particle trapping experiments, yellow-green (ex/em 505/515 nm) 1  $\mu$ m and 200 nm polystyrene particles (Invitrogen, Carlsbad, CA) were employed. The particle stock suspensions where diluted to a concentration of 1  $\times$  10<sup>7</sup> and 1  $\times$  10<sup>10</sup> microspheres/ml respectively, in deionized water with a conductivity of 0.5  $\mu$ S/cm and pH of 6.5.

Methods. The experiments were carried out using a ZEISS AxioVert A1 inverted microscope and the fluorescence filter # 49 (Carl Zeiss Microscopy, Thornwood, NY) equipped with a high-speed camera, used to capture microscopy pictures. A high voltage sequencer model HVS6000D (LabSmith, Livermore, CA) was used to apply DC voltages with platinum wire electrodes. For all dielectrophoretic experiments, images were captured five seconds after voltage application to allow enough particles to be trapped in the device. A Matlab 2015b (MathWorks Inc., Natick, MA) routine was used to perform fluorescence analysis from the images obtained with the high-speed camera. Further information on this process is included in the Supporting Information file (Figure S2). Fluorescence analyses were carried out in triple repetition, and results are included in Figures 3 and 4.

# ■ RESULTS AND DISCUSSION

**Electric phenomena.** COMSOL *Multiphysics* simulations were used to study the spatial distribution of the electric potential  $(\varphi)$ , electric field (E), and gradient of the electric field square  $(\nabla |\mathbf{E}|^2)$  through the microfluidic devices. To obtain a quantitative measure of these fields, a 10-mm-long cutline was defined in each channel design to pass through the gap between two consecutive rows of insulating posts. This cutline is illustrated in yellow in Figure 1a. Then, the magnitudes of  $\varphi$ , E, and  $\nabla |\mathbf{E}|^2$  along the cutline (considering its left end as the x=0 coordinate) were plotted in Figures 2a-2c, respectively.

The electric potential distribution for each microfluidic device considered in this study is illustrated in Figure 2a. From the plot, it is evident that each design produces a unique spatial distribution of  $\varphi$ . There are two interrelated aspects that deserve to be highlighted from this plot. The first one is the different number of slopes (voltage drops) exhibited by each

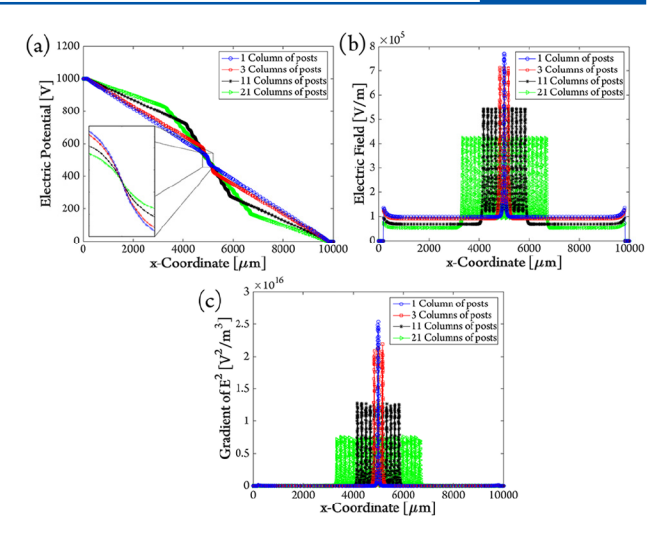


**Figure 2.** Distribution of the (a) electric potential, (b) electric field, and (c) gradient of the electric field square across the microchannel length. The inset in (a) illustrates the slope of the electric potential drop for the four different channel designs.

curve. This is clearly a result of the different number of posts columns in each microfluidic design. Introducing a larger number of columns in a design translates into a larger number of voltage drops within the channel. The second aspect to remark about Figure 2a refers to the steepness of the slopes in each curve. The curve associated with the device featuring a single column of posts exhibits a negative slope across the column. This slope is steeper than each individual slope present in the curve associated with the device featuring twenty-one columns of posts (see inset in Figure 2a). This can be explained from the fact that the total difference in electric potential across each microfluidic device is 1000 V; however, the total number of resistors (columns of insulating posts) in each device is different. Since this configuration can be represented as a series combination of resistors, as shown in Figure 1b, Kirchhoff's loop rule supports these observations.<sup>29</sup> The current generated in the system was measured experimentally using our voltage sequencer for this purpose. Since the resistance across a resistive element can be calculated as  $R = \Delta V/I$ , the measured current was used to calculate the equivalent resistance of the device for each design. The resulting values are  $R_{eq_1} = 138.3$ M $\Omega$ ,  $R_{eq_3}=152.4$  M $\Omega$ ,  $R_{eq_{11}}=169$  M $\Omega$ , and  $R_{eq_{21}}=187.5$  M $\Omega$ , supporting our hypothesis, where the subindex indicates the number of columns of insulators (for details, see Figure S3, Supporting Information file).

Since the electric field is defined as the negative gradient of the electric potential, it was expected that the devices featuring a larger number of columns exhibited weaker electric field magnitudes than devices with fewer columns. The magnitude distribution of E is depicted in Figure 2b, where a difference in magnitude of approximately 4  $\times$   $10^5$  V/m can be observed between the maximum measurement obtained for the devices with one and twenty-one columns of posts. At both ends of the plot, low-magnitude electric field peaks can be observed. These peaks are due to the electrode/fluid interface present in those regions of the channel.

Finally, the distribution of  $\nabla |\mathbf{E}|^2$  is depicted in Figure 2c. Since this parameter is directly proportional to the dielectrophoretic force, this plot predicts that including less

insulating posts columns in a microfluidic design will translate into a stronger dielectrophoretic force acting on any suspended particle of interest. It can be seen that a difference of approximately  $1.7\times10^{16}~{\rm V^2/m^3}$  exists between the maximum values of the curves corresponding to the devices with one and twenty-one columns of posts. This represents an approximate 312% increase in the magnitude of the dielectrophoretic force, allowing to decrease the trapping voltage required for some particles of interest or to trap elusive particles with no significant increase in voltage requirements.

Particle capture as a function of number of insulating posts. The findings obtained with COMSOL *Multiphysics* simulations were tested experimentally employing 1  $\mu$ m polystyrene particles. Figure 3 contains images illustrating

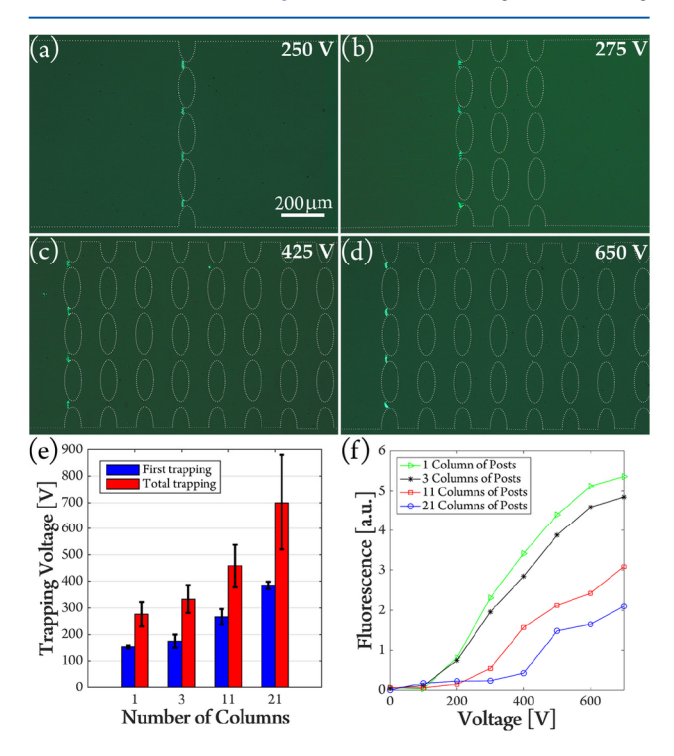


**Figure 3.** Images of dielectrophoretic trapping of 1  $\mu$ m particles in all four designs: (a) 1 column at 250 V, (b) 3 columns at 275 V, (c) 11 columns at 425 V, (d) 21 columns at 650 V, (e) electric potential difference required for initial and total particle trapping, and (f) fluorescence measurements of trapped particles in all four designs, at different applied voltages.

particle trapping as well as assessments on the particle enrichment obtained and the voltage required to trap particles in each design. Figures 3a–3d clearly demonstrate that there is a significant dependence of the electric potential difference required to achieve particle trapping on the number of columns of insulating posts in the channel. The same degree of dielectrophoretic particle trapping is obtained in all four designs at distinct applied voltages ranging from 250 to 650 V, which is a significant variation. These experimental results further strengthen the prediction made with the mathematical model: significantly greater dielectrophoretic forces are obtained in microchannels with lower number of columns of posts.

To further assess the differences between the four channels designs, experimental measurements were carried out to determine the electric potential difference required to achieve

"first trapping" and "total trapping" of particles with iDEP. The first trapping 2 event is defined as the experimental conditions at which DEP begins to capture some particles at the gaps in a column of posts while other particles keep flowing through (i.e., when DEP is still not the dominant particle transport mechanism), while total trapping occurs when no particle is able to escape from a well-defined band of dielectrophoretically captured particles (i.e., when DEP becomes the dominant particle transport mechanism). The shape of this band of particles is determined by both electrokinetic (EK) and DEP forces. 11 It is important to consider that the electroosmotic flow (EOF) velocity is directly proportional to the magnitude of E, and since the distribution of E depends on the number of columns of posts (Figure 2b), the EOF velocity at the constriction regions increases as the number of columns of posts decreases. However, since DEP has a second order dependence on E, DEP is the dominant effect and particle trapping is achieved at lower applied voltages as the number of columns of post decreases. Figure 3e illustrates the results on particle trapping, whereas expected from our modeling and experimental results, much lower applied voltages are required with less columns of insulating posts. The voltage range is significant; for example, for total trapping the applied voltages range from 276 to 700 V, that is an increase of 253%. This result is in close agreement with the 312% in the magnitude of dielectrophoretic force (expressed as  $\nabla |\mathbf{E}|^2$  in Figure 2d) predicted by our COMSOL model.

An assessment of trapping intensity vs applied voltage can be observed in Figure 3f. This figure clearly illustrates that the accumulation of particles is the lowest in the design with 21 columns of posts and it increases by 250% as the number of columns in the design decreases to 1. It is important to note that at very high voltages (>700 V), the system behavior might become anomalous when the microchannel has been used multiple times. At this point, particle trapping is no longer stable for all tested devices, possibly due to pH changes, electrolysis, and Joule heating, combined with wear by repeated testing of the devices at high electric fields. The results in Figure 3 reiterate the findings obtained with our COMSOL model and experiments.

Application: enabling the dielectrophoretic capture of nanoparticles. To further demonstrate the benefit of optimizing the post array design, we tested all four designs with 200 nm particles. Manipulation of nanobioparticles such as proteins, DNA, virus, and cell organelles is an area of high interest, as it can lead to the development of platforms for biomarkers enrichment and sensing. The ability to effectively handle nanosized particles can open applications for iDEP in the clinical and biomedical fields. <sup>33</sup> However, the high voltages required to manipulate nanoparticles have dampened its progress. For instance, voltages as high as 3000 V for polystyrene particles and 4000 V for PEGylated proteins have been reported for dielectrophoretic manipulation in traditional iDEP designs. 30,31,34 Figure 4a illustrates that significant dielectrophoretic capture of 200 nm particles can be obtained at applied voltages of 600 V by simply using one column of insulating posts. Figures 4b-4d depict how the particle trapping reduces as the number of columns of posts is increased. At 600 V, the degree of particle trapping ranges from substantial (1 column, Figure 4a) to negligible (21 columns, Figure 4d). These results are as expected considering the modeling and experimental results obtained with 1  $\mu$ m particles (Figure 3). Furthermore, the decrease in voltage requirements

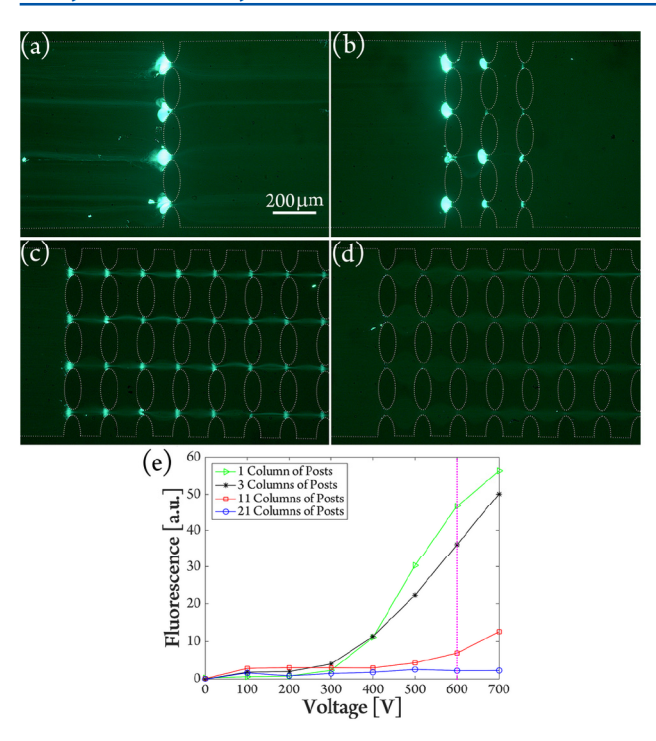


**Figure 4.** Dielectrophoretic trapping of 200 nm particles at 600 V in all four designs: (a) 1 column, (b) 3 columns, (c) 11 columns, (d) 21 columns, and (e) fluorescence measurements for a voltage sweep from 0 to 700 V; the magenta dotted vertical line at 600 V indicates the voltage where images (a) to (d) were taken.

is considerable when compared to similar reported systems where nanoparticle trapping occurred at  $\sim\!3000~\rm{V.}^{31,34}$  Particle trapping in Figure 4a was achieved employing only 20% of the voltage used in similar systems.  $^{31,34}$ 

The fluorescence analysis in Figure 4e clearly demonstrates that the design with only one column of posts has better performance in terms of particle trapping than the other three designs for the entire range of applied voltages studied. Particle trapping is significantly weaker in the more traditional designs with 11 and 21 columns of posts. These results are encouraging, as it is shown that the dielectrophoretic trapping of challenging nanoparticles is now possible at much lower applied voltages than previously reported. 29,30 By simply tailoring the system design, the particle trapping capabilities of the system are enhanced while voltage requirements are reduced, enabling the trapping and detection of valuable nanoparticles. Also, sample temperature rise will be smaller as a result of a reduction in stimulation voltage. This will benefit experimental work with delicate bioparticles, such as mammalian cells, reducing the risk of cell death. .

## ASSOCIATED CONTENT

# **S** Supporting Information

The Supporting Information is available free of charge on the ACS Publications website at DOI: 10.1021/acs.analchem.8b00139.

All channel design illustrations (Figure S1), Table S1 with domain and boundary conditions used with COMSOL, description of fluorescence analysis process (Figure S2), and a description of equivalent resistances estimation (Figure S3) (PDF)

#### AUTHOR INFORMATION

#### **Corresponding Author**

\*Phone +1 (585) 475-2773. E-mail: bhlbme@rit.edu.

#### ORCID ®

Blanca H. Lapizco-Encinas: 0000-0001-6283-8210

## **Author Contributions**

<sup>†</sup>V.H.P.-G. and R.C.G.-V. contributed equally.

#### **Notes**

The authors declare no competing financial interest.

#### ACKNOWLEDGMENTS

The authors would like to acknowledge the financial support provided by the National Science Foundation (Award CBET-1705895). This work was also financially supported by the Sensors and Devices Research Group of Tecnologico de Monterrey (002EICII01).

## **■** REFERENCES

- (1) Pethig, R. J. Electrochem. Soc. 2017, 164, B3049-B3055.
- (2) Crowther, C. V.; Hayes, M. A. Analyst 2017, 142, 1608-1618.
- (3) Mohammadi, M.; Madadi, H.; Casals-Terré, J.; Sellarès, J. Anal. Bioanal. Chem. 2015, 407, 1–12.
- (4) Soltanian-Zadeh, S.; Kikkeri, K.; Shajahan-Haq, A. N.; Strobl, J.; Clarke, R.; Agah, M. *Electrophoresis* **2017**, *38*, 1988–1995.
- (5) Ding, J.; Woolley, C.; Hayes, M. A. Anal. Bioanal. Chem. 2017, 409, 6405-6414.
- (6) Bhattacharya, S.; Chao, T.-C.; Ariyasinghe, N.; Ruiz, Y.; Lake, D.; Ros, R.; Ros, A. Anal. Bioanal. Chem. **2014**, 406, 1855–1865.
- (7) LaLonde, A.; Romero-Creel, M. F.; Lapizco-Encinas, B. H. *Electrophoresis* **2015**, *36*, 1479–1484.
- (8) Masuda, T.; Maruyama, H.; Honda, A.; Arai, F. PLoS One 2014, 9. e94083.
- (9) Luo, J.; Abdallah, B. G.; Wolken, G. G.; Arriaga, E. A.; Ros, A. *Biomicrofluidics* **2014**, *8*, 021801.
- (10) Jones, P. V.; Huey, S.; Davis, P.; McLemore, R.; McLaren, A.; Hayes, M. A. *Analyst* **2015**, *140*, 5152–5161.
- (11) Saucedo-Espinosa, M. A.; Lapizco-Encinas, B. H. Electrophoresis 2015, 36, 1086–1097.
- (12) LaLonde, A.; Gencoglu, A.; Romero-Creel, M. F.; Koppula, K. S.; Lapizco-Encinas, B. H. *J. Chromatogr. A* **2014**, 1344, 99–108.
- (13) Saucedo-Espinosa, M. A.; Lapizco-Encinas, B. H. J. Chromatogr. A **2015**, 1422, 325–333.
- (14) Pesch, G. R.; Du, F.; Baune, M.; Thöming, J. J. Chromatogr. A **2017**, 1483, 127–137.
- (15) Pesch, G. R.; Kiewidt, L.; Du, F.; Baune, M.; Thöming, J. *Electrophoresis* **2016**, *37*, 291–301.
- (16) Kwon, J.-S.; Maeng, J.-S.; Chun, M.-S.; Song, S. Microfluid. Nanofluid. 2008, 5, 23-31.
- (17) Weiss, N. G.; Jones, P. V.; Mahanti, P.; Chen, K. P.; Taylor, T. J.; Hayes, M. A. *Electrophoresis* **2011**, *32*, 2292–2297.
- (18) Jen, C.-P.; Chen, T.-W. Microsyst. Technol. 2009, 15, 1141-
- (19) Jen, C.-P.; Chen, T.-W. Biomed. Microdevices 2009, 11, 597-607.
- (20) Prabhakaran, R. A.; Zhou, Y.; Patel, S.; Kale, A.; Song, Y.; Hu, G.; Xuan, X. *Electrophoresis* **2017**, *38*, 572–579.
- (21) Nakano, A.; Luo, J.; Ros, A. Anal. Chem. 2014, 86, 6516-6524.
- (22) Gallo-Villanueva, R. C.; Sano, M. B.; Lapizco-Encinas, B. H.; Davalos, R. *Electrophoresis* **2014**, *35*, 352–361.
- (23) Cummings, E. B.; Singh, A. K. Anal. Chem. 2003, 75, 4724–4731.
- (24) Jones, T. B. *Electromechanics of Particles*; Cambridge University Press: New York, USA, 1995; p 265.
- (25) Ramos, A.; Morgan, H.; Green, N. G.; Castellanos, A. J. Phys. D: Appl. Phys. 1998, 31, 2338.
- (26) Green, N. G.; Ramos, A.; Morgan, H. J. Phys. D: Appl. Phys. **2000**, 33, 632-641.

(27) Baylon-Cardiel, J. L.; Lapizco-Encinas, B. H.; Reyes-Betanzo, C.; Chávez-Santoscoy, A. V.; Martínez Chapa, S. O. *Lab Chip* **2009**, 9, 2896–2901.

- (28) Morgan, H.; Green, N. G. AC Electrokinetics: Colloids and Nanoparticles; Research Studies Press LTD: Hertfordshire, England, 2003; p 324.
- (29) Perez-Gonzalez, V. H.; Gallo-Villanueva, R. C.; Camacho-Leon, S.; Gomez-Quiñones, J. I.; Rodriguez-Delgado, J. M.; Martinez-Chapa, S. O. *IET Nanobiotechnol.* **2016**, *10*, 263–275.
- (30) Mata-Gomez, M. A.; Perez-Gonzalez, V. H.; Gallo-Villanueva, R. C.; Gonzalez-Valdez, J.; Rito-Palomares, M.; Martinez-Chapa, S. O. *Biomicrofluidics* **2016**, *10*, 033106.
- (31) Romero-Creel, M.; Goodrich, E.; Polniak, D.; Lapizco-Encinas, B. *Micromachines* **2017**, *8*, 239–253.
- (32) Gencoglu, A.; Camacho-Alanis, F.; Nguyen, V. T.; Nakano, A.; Ros, A.; Minerick, A. R. *Electrophoresis* **2011**, 32, 2436–2447.
- (33) Zhao, K.; Li, D. Sens. Actuators, B 2017, 250, 274-284.
- (34) Saucedo-Espinosa, M. A.; Rauch, M. M.; LaLonde, A.; Lapizco-Encinas, B. H. *Electrophoresis* **2016**, *37*, 635–644.